Version of Record: https://www.sciencedirect.com/science/article/pii/S2214860420306059
Manuscript_b95837025deec9645a75e8ee151a8b14

Printing Polymer Blends Through *in situ* Active Mixing During Fused Filament Fabrication

*Zachary C. Kennedy and Josef F. Christ**

National Security Directorate, Pacific Northwest National Laboratory, P.O. Box 999, Richland, WA 99352, USA.

Email: * josef.f.christ@pnnl.gov

Abstract

Fused filament fabrication (FFF) enables production of 3D objects over a range of material compositions at low-cost relative to traditional manufacturing approaches. To date, a limited but growing number of materials are able to be used with FFF, however many applications exist where specific mechanical, thermal, or chemical properties are needed that cannot currently be met with the available feedstock selection. Therefore, a need exists to tune these materials for specific chemical or mechanical properties. One common formulation strategy to address these demanding design parameters is to develop composites or polymer blend filaments. Typically, this is a time-consuming and costly optimization process. Here, we have developed hardware for reproducibly mixing two filaments of similar or dissimilar compositions at the time of printing within individual printed layers. This mixing occurs via software-controlled rotating hardware in the chamber of an extruder's hot-end. The efficiency of mixing within the printed layers has been characterized in detail as a function of the rotational speed and geometry of the blending hardware. These parameters were exploited to program the ratio and distribution of thermoplastic-based filaments blended within printed extrudate. Example printed specimens were produced with thermoplastic

polyurethane (TPU) elastomer blended with rigid polylactic acid (PLA) and Nylon blended with PLA. In addition, a conductive carbon nanotube (CNT)-PLA composite was blended as a function of mixer geometry and input feed ratios with non-conductive PLA and resistance values were measured across the resulting printed specimens.

Keywords: material extrusion; in-situ blending; active mixing; polymer composites; multi-material printing

1. Introduction

Additive manufacturing (AM) has grown rapidly in both the industrial and research sectors as a means for producing functional parts with high complexities and unique form factors. Relative to traditional manufacturing approaches, AM methods offer the advantage of generating less material waste and being more receptive to an iterative design and fabrication process.[1, 2] One such AM technology, Fused Filament Fabrication (FFF), is popular due to its compatibility with a wide range of shelf-stable material feedstocks, simple operation, and for its very low cost. FFF utilizes thermoplastic-based feedstocks where it is standard to print with commodity polymers such as acrylonitrile butadiene styrene (ABS), polylactic acid (PLA), and polyamides (e.g Nylons). Recently, commercially available high-performance FFF feedstocks have been introduced by companies such as 3DXTech, including homopolymers polyetheretherketone (PEEK) and polyphenylene sulfide (PPS). Composites such as carbon-fiber reinforced-thermoplastic (e.g. from 3DXTech)[3] and metal filled polymer (e.g. Stainless Steel 316L, Al, Cu from Markforged and the Virtual Foundry) are also now available as feedstocks.[4] The development of new “designer” or advanced functional FFF-compatible materials is anticipated to remain central to further growth and application of the technology going forward.[2]

Several strategies are currently used to tune FFF material compositions to alter printing performance and affect the resulting part's utility after printing. FFF-compatible polymers are often processed with additives (e.g. lubricants, antioxidants, plasticizers) to modulate rheological, thermal, and mechanical properties.[5] More advanced and stimuli-responsive objects obtained from a FFF process may derive from composite feedstocks[6] that incorporate fillers such as inorganic particles or nanomaterials,[7, 8] fluorescent material,[9] non-thermoplastic macromolecules,[10] involve multiple thermoplastics,[11], or involve irreversible thermal strain for shape memory.[12] Each new composite or blended filament requires significant optimization and thus it may be costly and time-consuming to make compositional changes at scale in an iterative fashion. Commercially, many FFF feedstocks have complex chemical compositions and this effort and engineering cost is implied, for example, by the use of proprietary trade names to protect the specific composition of the material. Approaches modeling the extrusion flow and heat transfer processes have been recently reported aimed at reducing the complexity of iterative materials design for FFF feedstocks as detailed by Gilmer et al. [13] and D'Amico and Peterson.[14]

Alternatively, more complex printed structures may be produced by printing with FFF machines that possess print heads with unique capabilities. For example, multi-extrusion print heads (capable of extruding multiple filaments) are valuable to print sacrificial supporting features that are removed or dissolved post-print[15] or to print with several different feedstocks to achieve functionally-graded structures.[16] One type of print-head design that has garnered interest is often termed a mixing nozzle, where the print-head is designed to have multiple inputs feeding into a single melting chamber followed by extrusion out of a single nozzle. This, in theory, allows for the printing of multiple filaments in tandem and has been recently investigated

to some extent. For example, through tandem polymer extrusion, color mixing is possible with hardware such as the Diamond Hotend by RepRap for RGB color[17] or the in-development Rova4D Full Color printer by ORD Solutions for CMYK+white color.[18] However, a shortcoming of existing mixing nozzles is that there is rarely ever true homogeneous mixing of the polymers due to high viscosity resulting in laminar flow. While this may be sufficient for color mixing, similar to how a dot-matrix printer would approximate colors, it is not adequate for situations where greater polymer blending is required, particularly if those polymers are of dissimilar compositions. In these color mixing extrusion systems, the feedstocks are derived from the same parent polymer material, combining two colors of PLA, for example. Beyond simple color mixing or complex multimaterial printing by direct ink writing of viscoelastic inks,[19, 20] FFF printing with two dissimilar thermoplastics through one nozzle was described previously by employing a bi-extruder with a static intermixer.[21] A further development by the same group described extrusion of two mechanical interlocked immiscible polymers using the static intermixer insert in a multi-material system. [22] This design enabled printing of a functionally graded soft robotic gripper. Some passive mixing of the input polymers occurred with this static intermixer implementation. An additional study designed and produced functionally graded objects by FFF through the use of a two input to one output hot-end where the individual components in the printed extrudate were side by side (i.e. with no mixing) in each layer. [23] To our knowledge, an extruder capable of more active and systematic mixing of multiple input filaments has yet to be reported.

In this article, we detail the development of hardware for active mixing of two FFF feedstocks at the time of printing within individual printed layers with high efficiency. This work focused on the blending of filaments with mechanically or functionally dissimilar compositions.

The mixing extruder hardware introduced was designed for compatibility with commonly used low-cost FFF 3D printer styles and required minimal modifications for implementation. Further goals of this study were as follows: 1. determine the process and design parameters to predictably distribute the two input filaments in a variety of arrangements within the printed extrudate; 2. enable the ability to program the ratio of the two filaments being blended; 3. interface the hardware with the slicing software for simple control of the system.

2. Hardware Design and Experimental

2.1 Printing Hardware and Experimental Setup

The printer used in this work was a modified Printrbot Simple Pro, running an Azteeg X3 pro control board with custom Repetier firmware. Repetier firmware was selected as it allowed for ratioed control of the extruder stepper motors which provides for material flow adjustment to tune the mixing ratios. The hot-end heater block is a custom fabricated solution comprised of two inputs and a single output. A third, non-filament, input exists to allow for the insertion of a mixing element to be run down the length of the melting chamber. The hot-end is comprised of six components: the custom heater block, two E3D V6 heat breaks and associated heat sink, the mixing element, the mixing element gasket, and a standard brass nozzle (Figure 1a). The PTFE mixing element gasket was used to prevent leakage between the rotating mixer element and the melt-chamber. A detail drawing of the hot-end is provided in the supplementary information file (Figure S1). By implementing a separate stepper motor to operate the mixing element, one can control the polymer feed rate and mixing element velocity independent of each other. Further, by connecting the mixing element stepper motor to the printer's controller board, the mixing rate can be operated such that it maintains proportional mixing speeds to the polymer flow rate. As such, the tunable parameters of the mixing nozzle are: polymer flow rate, input polymer ratio,

and mixing element speed. The mixing element can be replaced with differing geometries to alter the mixing behavior. Three mixing geometries were examined in this study: a smooth rod (SR), drill bit (DB), and reamer bit (RB). A control was also used throughout the study where no mixer element (NM) was present. A schematic of the tunable parameters and geometries of the mixing elements are depicted in Figure 1b while Figure 2 provides a more detailed illustration of the mixing element geometries.

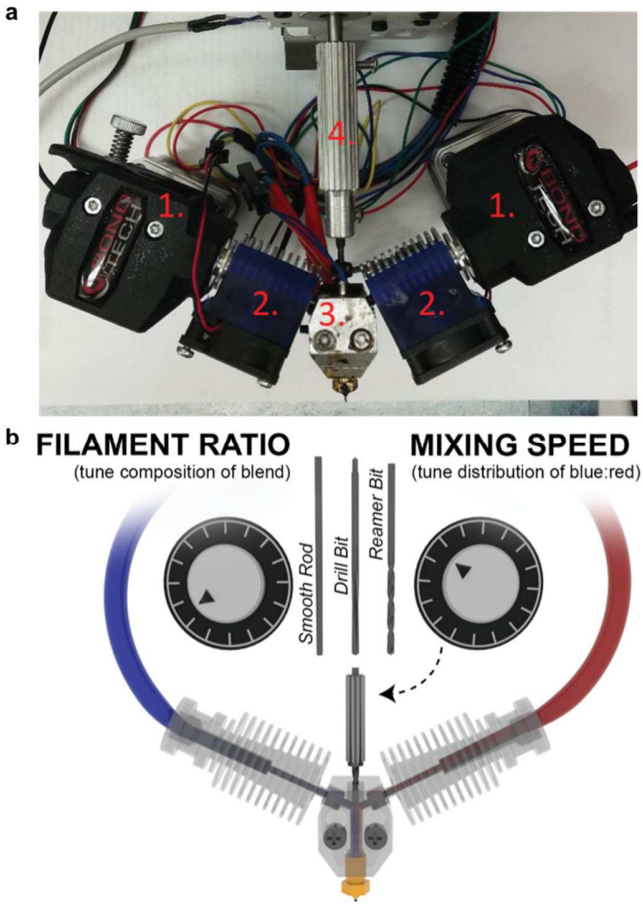

Figure 1. (a) Photograph of the primary components of the two-filament mixing extruder where the filament drive mechanisms (1), heatsinks (2), heater block (3), and mixing element (4) are labeled. (b) Schematic illustrating the programmable parameters and the mixing element designs examined in this study.

2.2. Materials and Printing Methods

The FFF filaments used as input materials in this study were purchased with a nominal diameter of 1.75 mm and were used as received from the following suppliers: Semiflex thermoplastic polyurethane (TPU, midnight color, Shore hardness = 98A or 50D) from Ninjatek (Manheim, PA, USA); PRO series red color polylactic acid (PLA), PRO series black Nylon from Matterhackers (Foothill Ranch, CA, USA), and Conductive PLA containing carbon nanotubes (CNT-PLA) (FE-PLA-0750, black color) with a manufacturer reported volume resistivity of 0.75 ohm cm from Functionalize Inc. (Seattle, WA, USA). Samples were printed through 400 μm brass nozzles, onto the Printrbot Simple Pro bed with the exception of Nylon/PLA samples as noted below.

All TPU/PLA blends were printed with a hot-end temperature of 230 °C onto a bed heated to 55 °C. The CNT-PLA/pure PLA blends were printed with a hot-end temperature of 215 °C onto a bed heated to 55 °C. All tensile samples were printed with a maximum speed of 20 mm/s. Samples were printed at 300 μm layer heights with an extrusion width of 400 μm. The parallel and perpendicular samples were printed with a rectilinear infill pattern at 100% infill, no external shells. The infill was set to not alternate every layer, with the parallel samples infill in-line with the tensile samples' major axis and the perpendicular samples' infill in-line with the minor axis. Nylon/PLA blends were printed with a hot-end temperature of 230 °C as single-strand extrudate samples, not printed onto the bed, and rather were collected directly after exiting from the print nozzle. For mechanical testing, tensile bar samples were printed in two orientations. One orientation consisted of a printed raster pattern perpendicular to the direction of

tensile loading and the other orientation consisted of a printed raster pattern parallel to the tensile loading. The tensile bar samples were designed to the Type 1BA dogbone dimensions according to ISO-527 standard.[24]

2.3. Materials Characterization

Thermogravimetric analysis (TGA) was recorded on printed extrudates using a Netzsch TG 209 F3. Sections of samples (typically 15 mg) were placed in an Al_2O_3 pan and analysis was performed from 40 – 800 °C at a ramp rate of 5 or 10 °C/min under a flowing air atmosphere. Temperature ramp rates are indicated for specific blends in the figure captions. Derivative thermogravimetry (DTG) curves were produced from calculation of the first derivative of the TGA weight loss curves.

Optical photographs of printed extrudate materials were recorded using an Olympus BX51 Microscope equipped with a DP80 color camera (Olympus). Small lengths of sample (~1 cm sections) were sectioned with a razor blade from various points along a longer length of extrudate (with ~20 cm gap in between sections) and mounted vertically within a plastic cylindrical cavity affixed to a glass slide. Dark-field images were then recorded with top-down illumination of the sample's cross section. In the blended specimens containing elastomer, some macrostructural deformation may have resulted in the extrudate due to cutting at room temperature. However, deformation from this cutting procedure was not expected to affect conclusions made related to the distribution of the two phases.

Tensile testing was carried out according to ISO-527 standard protocols [24] on a Mark-10 ESM 303 test stand with digital force gauge at a rate of 15 mm/min. The ultimate tensile strength (UTS) and Young's Modulus (YM) values were determined by measuring the nominal stress and strain, where engineering stress is calculated as:

$$\sigma_n = \frac{F}{A}$$ Eq. 2.1 [24]

Where F is the measured tensile load and A is the measured cross-sectional area, and the engineering strain is calculated as:

$$\varepsilon_n = \frac{l}{l_i}$$ Eq. 2.2 [24]

Where l is the measured displacement and l_i is the initial length. To characterize the electrical properties of the mixed CNT-PLA/PLA blends, resistance measurements were performed by printing modified dogbone samples (4 cm in length, 1.5 mm thick) for the specified compositions listed in Table 2. Sample dimensions are given in the supplementary information (Figure S3). A two-part silver conductive epoxy adhesive (MG Chemicals 8331) was applied to the grip sections on each dogbone and cured as directed by the manufacturer to minimize contact resistance. Two-point resistance was recorded with a multimeter (Fluke 187) on three separate dogbones for each composition and mixing condition listed. Average resistance values with error bars are provided per cm length.

3. Results and Discussion

3.1. General approach and overview of FFF mixing extruder development

In this work, the ability to induce mixing of two input FFF filaments at the time of printing through the use of a rotating ("active") mixer element was investigated in detail. Prior to discussion of the printed blend samples produced, we first consider how material is extruded on a FFF system. Typical FFF systems are comprised of a 3-axis motion gantry system and print head. It is often in the print head assembly where significant research and opportunity for improvement exists. All FFF print heads consist of a feeding mechanism, often called the extruder, and a melting chamber, usually referred to as the hot-end. While the extruder and hot-

end can vary significantly between manufacturers, they all provide the essential function of providing the driving force for the polymer and the means of melting and extruding the polymer out of a nozzle.[25] Here, a custom hot-end was manufactured with two input filament feedthroughs and a third input where a mixing element is installed. The active mixing element is rotated via an attached Nema 17 stepper motor. The hot-end design allows simple exchange of mixing elements with different physical features and thus enabled screening of three different surface geometries of mixer: a smooth rod (SR), a drill bit (DB), and a four-fluted reamer bit (RB) (Figure 2). Characterization of the hardware design and process parameters implemented was performed on blends derived from TPU/PLA, Nylon/PLA, and CNT-PLA/pure PLA input filaments. Printed samples are referred to in the remainder of the paper by the geometry and applied rotational speed of the mixing element during printing. For example, DB-1000 indicates the use of a drill-bit mixer rotating at 1000 steps/mm. For clarification, when referring to steps/mm, the mixing element rotational velocity – or the steps per second of the driving stepper motor – is software controlled to maintain a proportional rotational velocity with respect to the filament input speed. That is, as the filament input slows or accelerates, so does the mixing element. For example, if 1.0 mm of filament is fed in, the mixing element will rotate 1000 steps when set to 1000 steps/mm. To achieve this control, the support code for mixing nozzles found within the Repetier firmware was used. Additionally, the configuration.h file is provided in the supplementary information.

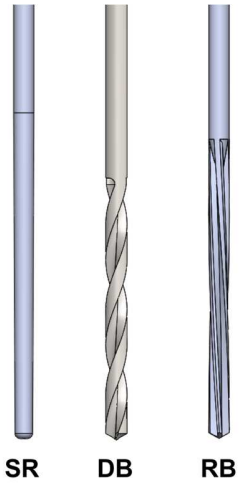

Figure 2. Schematic of the mixer designs implemented in the study.

3.2. Printed blends of TPU/PLA

Blends of TPU/PLA were printed to explore in detail the relationship between the mixing element geometry and applied rotational speed of the element and the resulting mixing achieved. Furthermore, the extent of polymer mixing and effect on the mechanical properties in printed objects was measured. FFF printed TPU/PLA objects, derived from filaments produced by traditional polymer blending techniques, are of interest, for example, as esophageal stents,[26] flexible strain sensors, [27] and as a potential scaffold for tissue engineering.[28] TPU filament used in this study, supplied as Semiflex by Ninjatek in Midnight (black) color, is a polyester polyurethane-based elastomer with a manufacturer reported elongation at break of 600%, Shore Hardness of 98A, and is typically printed with a hot-end temperature of 230 °C. Further mechanical properties of printed Semiflex TPU using open-source FFF printers were reported previously.[29] PLA filament, supplied in red color as PRO series grade by Matterhackers, is a rigid thermoplastic in comparison and has a recommended printing hot-end temperature of 205 ± 15 °C. Mixed TPU/PLA samples were printed at 230 °C hot-end temperature, well-below the thermal decomposition of PLA (refer to the TGA data) but high enough for appropriate feeding

of the TPU filament component. We note the selection of an extrusion temperature for a given blend of input filaments and desired composition could be further optimized in future application through 1) rheological analysis and 2) by a ensuring co-continuous structure is and may be obtained.[30]

During the screening of varying mixing element geometries and rotational speeds applied in TPU/PLA experiments, two separate metrics of mixing efficiency were considered. The first was to consider the extent to which two input filaments could be blended using the mixing extruder relative to literature examples where material was blended using a traditional processing technique such as by mechanical means in a compounder. In melt compounded and hot-press molded TPU/PLA blends, the two phases were reported to be partially miscible due to hydrogen bonding between the molecular backbones of each constituent polymer.[31] Despite the partial miscibility and thorough blending procedures employed, however, tens to hundreds of micron scale individual domains of the two polymers were observed in the blends across varying blend ratios. Similarly, a micron-scale phase separation was reported in other reports detailing more immiscibility in PLA/TPU blends, at most ratios prepared by traditional means without compatibilizers.[32-34] These studies are highlighted to articulate that a thoroughly-mixed blend of predominately immiscible input polymers while practically of value may still yield phase separated domains. More broadly, the solubility parameters (e.g. as outlined by Hildebrand) may be useful to predict miscibility in a set of blended polymers. However, this was not attempted given the unknown (i.e. proprietary) structure of the input TPU in this case. The second metric when assessing the mixing in this study was related to the ability to impart reproducible novel types of control over the degree of mixing during printing. For example, a blend with incomplete

mixing that subsequently yields distinct patterns of the two constituent phases would not be possible using more traditional polymer blending approaches.

3.2.1. Characterization of mixing as a function of mixing element geometry and rotational speed in printed (50:50)-TPU/PLA

Single-layer (50:50)-TPU/PLA blended extrudate samples rotating at 1000 steps/mm were initially produced and characterized by TGA to assess the ability of the software and hardware to correctly feed the target input ratio of the two filaments reliably. PLA and TPU components thermally degraded in both oxidizing (Figure 3, flowing air atmosphere) and inert (not shown, flowing He atmosphere) environments across similar temperature ranges. The convolution of the mass losses of the two constituent feedstocks in the blends made quantification of the actual ratios in the filaments not possible. However, the TGA traces of (50:50) printed blends obtained without a mixer and with each of the three mixer geometries screened were similar and suggest a similar composition was obtained in each blend. The rate of mass loss depicted in the DTG plot illustrates the similarities of the major mass transitions in more detail supporting that the blended compositions were similar in the prints. It was noted that the peak rates of mass loss shifted to higher temperatures in each of the "active" mixer designs compared to the no mixer control and was most pronounced in the **DB-1000** and **RB-1000** samples (Figure 3b, inset of the high-temperature decomposition region of TPU). The actively mixed samples also exhibited increased die swell at these mixer rotation speeds which was not present without mixing. The die swelling is expected to yield lower surface area printed material (associated with the increased diameter assuming a fixed surface morphology) and subsequently a decreased rate of mass loss of the constituent polymers shifting to higher temperature in the DTG). It is also conceivable that increased mixing leads to greater interaction at a molecular

level between PLA and TPU chains as has been reported previously[31] and therefore this interaction would enhance the thermal stability.

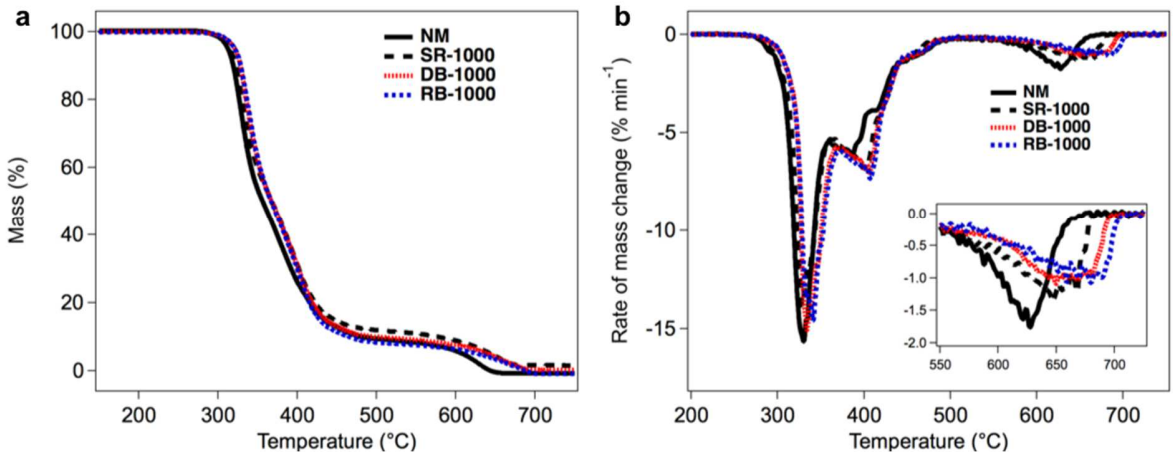

Figure 3. (a) TGA and (b) DTG data recorded (in air, 10 °C/min ramp rate) on single printed (50:50)-TPU/PLA strands as a function of mixing element design.

An apparent correlation between the mixing element geometry, its rotational speed, and the resultant extrudate swell was observed in the polymer extrudate. Figure 4 shows the printed extrudate diameter as a function of mixing element velocity for each of the tested element geometries. Extrudate swell increased as a function of speed and increased more rapidly with the inclusion of flutes on both the DB and RB mixing elements. Extrudate swell has been attributed to an increase in polymer melt flow velocity and an increase in polymer melt shear[35, 36] which indicates that the mixing element geometry could be tailored to influence secondary driving forces. Thermoplastic filaments are under high shear during a traditional FFF extrusion process which results in shear thinning (i.e. a reduced viscosity that enables printing). Furthermore, the shear is expected to be even more pronounced when using the active mixer designs. It was previously established in a model shear-thinning polystyrene that increased shear rates not only reduced viscosity but increased swelling ratios and corresponding extrudate diameters.[37] The

normal stress differences as a result of elasticity (i.e. recoverable shear) also play an important role.[38] Therefore, the increased extrudate swelling observed with the DB and RB mixing elements operating at the highest rotational velocities (>1000 step/mm) is believed to be a product of elevated shear rates and lower viscosities relative to the no-mixer and smooth rod element extrusion environments.

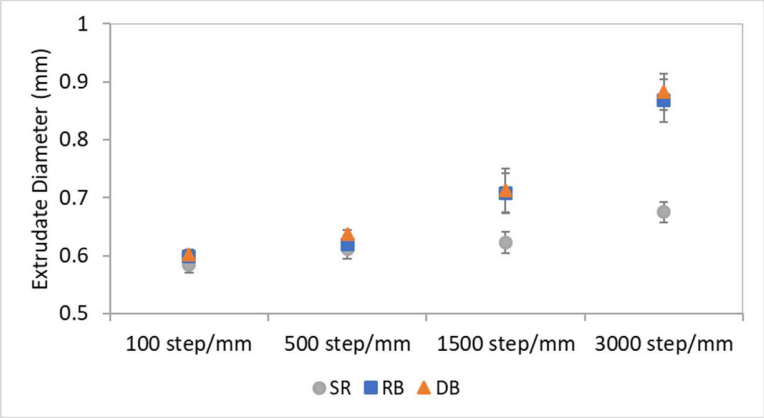

Figure 4. Extrudate diameter as a function of mixing element velocity and mixing element shape.

Optical images of the cross-section of resultant extrudates as a function of mixing element velocity for each of the three mixing element designs were recorded (Figure 5). The TPU and PLA filaments were blended while printing through a 400 µm nozzle resulting in ~600-900 µm diameter extrudate as a result of die swelling. A black-colored TPU and a red colored PLA were selected to provide optical contrast and quickly characterize the extent of blending. The cross-sectional distribution of the input feedstocks was observed in particular and consistent patterns based on the geometric design of the mixing element. Furthermore, as the rotational velocity of the mixer was increased, there was significant improvement in polymer mixing as the patterns become less pronounced. Visually, based on the 3000 steps/mm speed, the SR mixing element results in the poorest mixing and the DB and RB mixing elements result in the greatest

mixing. In the DB and RB samples, with moderate mixing at 1000 steps/mm, distinct black TPU domains remain. With greater mixing at 3000 steps/mm using the DB and RB, the blends have more completely merged by color with only minor distinct phase patterns at this resolution. One hypothesis regarding the improved mixing of the DB and RB mixers over the SR mixer is that, unlike the SR, the DB and RB provide alternating flow channels through the flutes of the mixer, with each flute alternating between each material input. Visually, this can be seen with the DB showing a distinctive 2-flute pattern in the cross section, while the RB shows a distinctive 4-flute pattern in the cross section, particularly when comparing the cross sections at the slow 100 step/mm rotation speed. While not a primary focal point of this research, it is notable that by adjusting the mixing element geometries and rotational speed applied, one could target a particular cross-sectional pattern or distribution of the two feedstocks in the polymer blend to tune material performance.

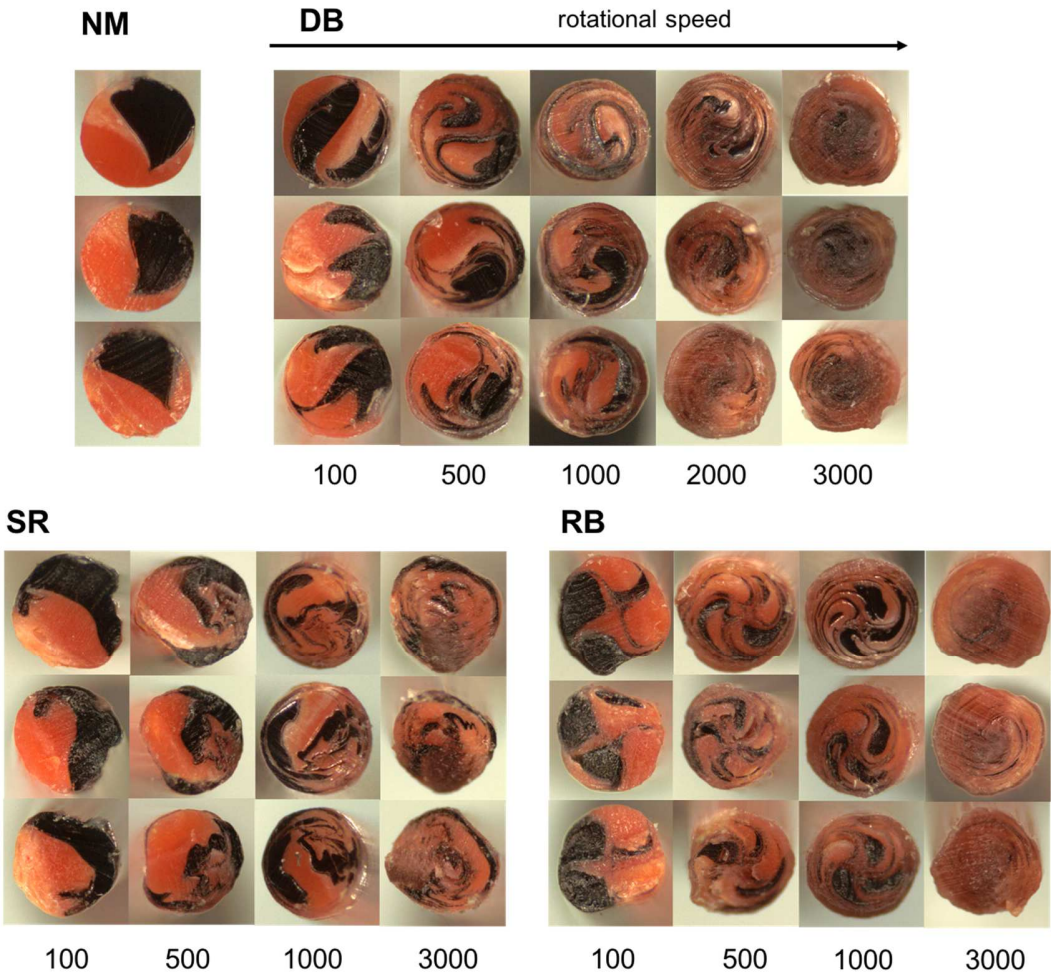

Figure 5. Cross-sectional optical images recorded to visualize the distribution of TPU (black) and PLA (red) within single printed strands (50:50 ratio, 400 µm diameter nozzle) as a function of mixer element design and rotational speed. Images of three separate sections of extrudate are provided to demonstrate consistency in the mixing behavior for a given set of hardware and conditions applied.

3.2.2. Effect of mixing element geometry on the mechanical properties of printed (50:50)-TPU/PLA

The influence of the mixer design and corresponding distribution of the TPU and PLA components on the resulting mechanical properties was determined. For this experiment, mixed

(50:50)-TPU/PLA tensile bar samples were printed with 400 μm resolution without a mixer and with each of the three mixer element designs rotating at a fixed speed of 1000 steps/mm. Tensile bars with each printing condition were printed with individual layers aligned parallel and perpendicular to the applied tensile stress (Figure 6). The average ultimate tensile strengths (UTS) and Young's modulus (YM) were calculated from tensile tests on five specimens per mixer design and print path (Figure 7, data tabulated in supplementary information). In comparing the results of the mixed samples to the unmixed sample, there is only a small change in mechanical performance. With respect to the parallel printed samples, the mixed samples show a mild increase in the UTS while the perpendicular samples show no indication that mixing improves or hampers the interlayer adhesion, at least with regards to TPU and PLA. This would seem to indicate that the primary driving force for interlayer adhesion between adjacent layers is not as influenced by the degree of mixing. Or perhaps, the material is behaving as a polymer composite and, at the time of the PLA failure, the load shock imparted to the TPU is enough to break it suddenly. This is plausible as the yield strength of the TPU is much lower than that of the PLA, according to the manufacturer. Figure 8a shows the stress-strain plot for the parallel printed samples showing that the unmixed sample failed more rapidly than the mixed samples. Furthermore, during tensile pulling, the unmixed samples demonstrated significant delamination and tearing in the parallel samples over the mixed samples. However, it appears to be an intralayer delamination of the individual extruded fibers. Visually (Figure 8b and Figure 8c), this was attributed to the PLA portion of the extruded strands failing before the TPU portions, unlike the mixed sample, which behaved more like a singular material throughout the pull test. While the samples may behave similarly in their bulk material properties, at the intralayer level, there is a significant difference in behavior between the mixed and unmixed samples.

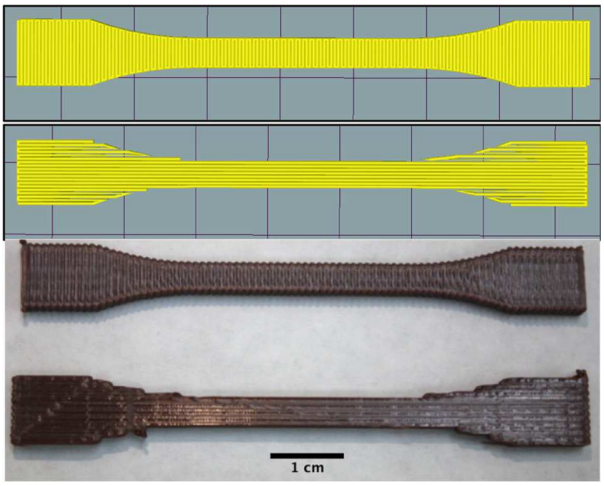

Figure 6. Designs (top) and photos (bottom) of (50:50)-TPU/PLA tensile bars printed with individual layers in a perpendicular and parallel to the applied tensile force.

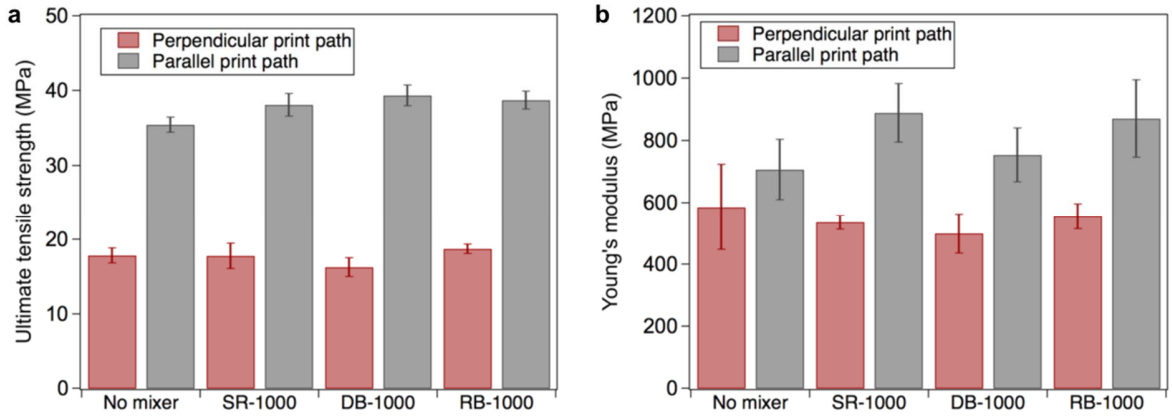

Figure 7. (a) Ultimate tensile strength and (b) Young's modulus of (50:50)-TPU/PLA tensile bar samples as a function of mixer type and print path

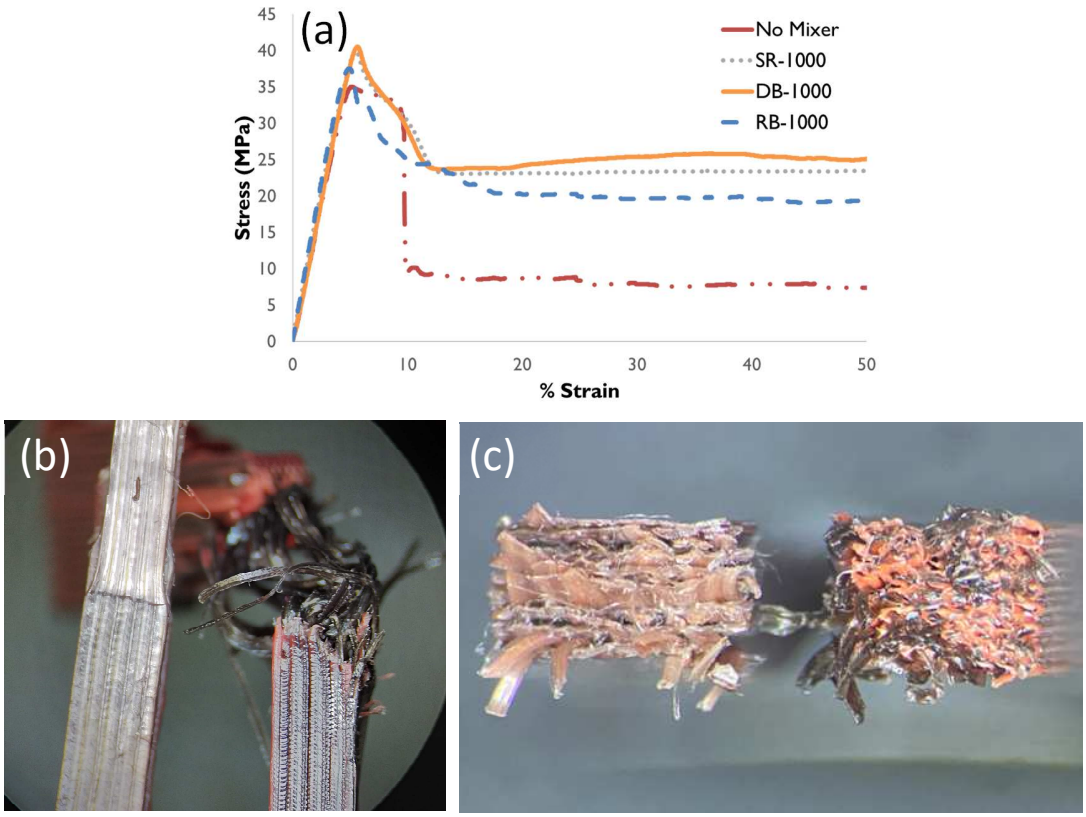

Figure 8. (a) Stress-strain plot of parallel printed samples and (b-c) optical images of post tensile-pulled DB-1000 (left) and NM (right) samples.

3.2.3. Tuning the composition in printed TPU/PLA and application of the blending method to tune composition in printed Nylon/PLA blends

The hot-end and mixing hardware was interfaced to the slicing software for fine control of not only the rotational velocity of the mixing element but also to enable seamless tuning of the blend composition by modulating the feed ratios of the input filaments. Single-layer printed TPU/PLA samples were produced using the DB-1000 mixer conditions over a wide range of compositions with input feed ratios programmed from (90:10)-TPU/PLA to (10:90)-TPU/PLA

(Figure 9a). It was readily apparent by eye that the blended material transitioned from black (from TPU) to brown to red (from PLA) as the ratio of the PLA increased in the sample. This suggests the actual composition achieved correlated with the programmed feed ratio of the two feedstocks. To further assess the composition obtained, TGA was performed on the printed TPU/PLA blends (Figure 9b) and pure printed sample controls. As described in the mixing efficiency section with (50:50)-TPU/PLA, the onset and primary thermal decomposition of the two constituent materials does overlap significantly. However, pure PLA degrades nearly completely (> 99.4 % mass loss) by 425 °C in these conditions, whereas the polyurethane structure of the pure TPU has a mass loss of 79.5 % by the same temperature. As the PLA concentration in the printed blends increased, the total mass loss increased accordingly at this temperature point in the analysis to provide support for compositional control. In future application, quantification of the composition of the blended extrudates could be performed using a technique such as selective solvent etching of one of the constituent phases.

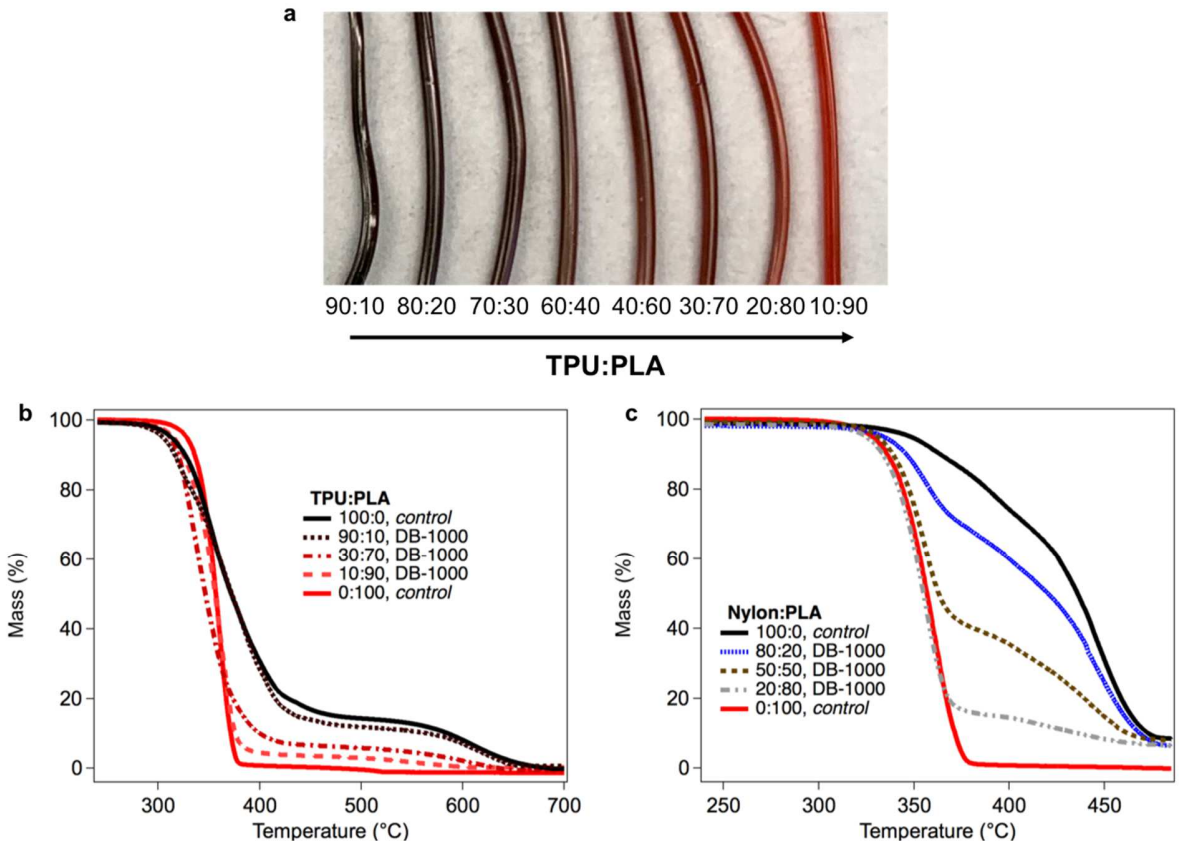

Figure 9. (a) Photos and (b) TGA data recorded (in air, 5 °C/min ramp rate) on single printed TPU/PLA strands as a function of TPU:PLA ratio and (c) TGA data recorded similarly on single printed Nylon/PLA strands as a function of Nylon:PLA ratio. In both sets of blends, mixed samples were prepared using the DB geometry with a rotational speed of 1000 steps/mm.

The mixing system was designed as a tool for direct blending of a wide array of filament feedstocks and to accelerate the production of FFF objects with new compositions and properties. To this end, the hardware was used to print blended Nylon/PLA materials using the DB mixing rotating at 1000 steps/mm (DB-1000). It was straightforward to apply the blending methodology detailed in the TPU/PLA samples to this second pair of feedstocks. The input feed ratio of the two components was tuned to produce samples with compositions from (80:20)-Nylon/PLA to (20:80)-Nylon/PLA. TGA analysis was used to monitor first the thermal

decomposition of PLA followed by the decomposition of the Nylon contained in the printed blends (Figure 9c). As these thermal transitions are less overlapped than the TPU/PLA samples, it was readily apparent the changes in Nylon/PLA composition programmed into the system were reflected in the actual printed samples.

3.3. Printed blends of CNT-PLA/Pure PLA: Effect of mixing efficiency on the conductivity of the blend

With the addition of an active mixing element, the notion of being able to adjust the ratio of input filaments becomes even more interesting when one considers the addition of a functionalized material as an input such as one with filler added. In this case, the addition of a semi-conductive filament input was tested in order to characterize how the mixing head interacts with functionalized, composite feedstocks. Table 2 outlines the relationship between mixing element geometry, speed, and the mixing behavior of a conductive PLA/pure PLA blend. In this case, the conductive PLA (Functionalize) uses multiwalled carbon nanotubes (MWCNTs) to imbue the PLA with semi-conductive properties (average two-point resistance = 53 ohm/cm in the materials produced here). Briefly, the addition of MWCNTs has been well characterized in providing electrical properties to polymers through the conductive network matrix produced by the MWCNTs.[39, 40] It has also been shown that the conductivity of the resulting composite polymer is highly influenced by both the orientation and dispersion of the MWCNTs.[41, 42] As can be seen, for the 50:50 mixtures, there is little change in the resistance except for the SR samples, which show a decrease in resistance of almost 2.6 times that of the unmixed samples. As the ratio biases towards the pure PLA in the (30:70)-CNT-PLA/pure PLA mixtures, the change in resistance becomes far more prominent. The SR samples once again show a decrease in resistance while the DB and RB samples show a significant increase in resistance.

Mixer Design	CNT-PLA / pure PLA feed ratio	Resistance (kohm / cm)	Mixer Design	CNT-PLA / pure PLA feed ratio	Resistance (kohm / cm)
No mixer	50:50	2.28 ± 0.13	**RB-1000**	70:30	0.35 ± 0.03
SR-1000	50:50	0.87 ± 0.14	**No mixer**	30:70	4.23 ± 0.95
DB-1000	50:50	2.19 ± 0.17	**SR-1000**	30:70	3.64 ± 0.40
RB-1000	50:50	2.01 ± 0.05	**DB-1000**	30:70	12.35 ± 2.99
No mixer	100:0	0.053 ± 0.001	**RB-1000**	30:70	29.41 ± 3.69

Table 2. Comparison of sample resistivity as a function of mixer design and feed ratio in printed CNT-PLA/pure PLA blends.

In the case of the SR mixer derived specimens, it is proposed the percolative MWCNT network within the polymer matrix is more preserved compared to the specimens processed by the RB and DB mixers. However, of particular interest is the increased conductivity of the SR specimens over the specimen obtained with no mixer. In the SR-1000 cross-sections, some homogenization has been initiated but the MWCNT phase is mostly continuous. Whereas in the no mixer cross-section, side-by-side extrusion is realized as is apparent in the cross-section images with more discrete separations (i.e. breaks) in the conductive matrix and a relatively higher resistance. In a 3-dimensional printed sample comprised of many layers and interfaces, it is envisioned the use of the SR-1000 setting provides optimal points of contact and preservation of continuous conductive network as compared to specimens processed by other settings. The DB and RB mixing elements both appear to be inducing far more dispersive mixing than the SR mixing element. Increased shear force (i.e. a more dispersive mixing environment) acting on the polymers has been shown to improve additive dispersion within polymer composites.[43] Based on the DB and RB results, it either indicates that the MWCNTs are being well dispersed into the

added, nonconductive PLA, or the MWCNTs are being oriented in a common direction, resulting in an overall decrease in the conductance of the mixed material.

4. Conclusions

In this paper, the design and implementation of new hardware capable of transforming two input filament feedstocks into a blend in the hot-end of an FFF printer is outlined. The hot-end mixing element hardware was designed to be compatible with standard FFF printers. By interfacing the hardware with the slicing software, a user is able to tune the rotational speed of the mixing element and input polymer flow rates simultaneously. Ultimately this control introduces a unique approach to systematically tune the polymer blend composition (i.e. ratio) and internal distribution of the two input materials within individual printed layers during a build. The capability of the hardware was demonstrated by the printing of mechanically, mixed blends where the two input polymers were different thermoplastics, specifically TPU/PLA and Nylon/PLA. The use of an active mixing extruder allowed for the efficient generation and screening of polymer composites with varying compositions and loadings of filler. To this end, MWCNT-doped PLA was blended with PLA at different ratios and with varying mixing element designs. Each of these parameters contribute to the resulting conductivity observed in the printed materials as a result of the amount and distribution of the MWCNTs present. Lastly, when using the mixing extruder setup with a single polymer only, the parts are of similar quality to those produced with a standard FFF extruder (refer to supplementary information Figure S2 for tensile test data).

Overall, this work illustrates the active blending of two input thermoplastic-based filaments directly in a single-step during a FFF printing process. More traditional development of a FFF blend or composite feedstock requires multiple steps where the desired composite is first

obtained by blending for example in a twin-screw extruder and spooled into filament prior to printing. Using drill-bit and reamer-bit mixer elements operating at high-rotational speeds, the two input phases were shown to be highly-mixed on a practical scale. However, it should be noted that the mixed polymer blends obtained by this *in situ* approach have yet to be directly compared to a rigorously mixed blend prepared by traditional means. Complete mixing in these cases is typically dictated by the miscibility or chemical interactions between the individual constituent components. A few potential trade-offs with using this active mixer system compared to a traditional extruder are: 1) the requirement of an available third stepper driver to operate the mixing element and 2) the increased weight and footprint as it currently stands. The first trade-off is a result of common printer controller boards not offering a sufficient number of drivers. Broadly speaking, an *in situ* material blending approach is envisioned to accelerate the iterative development cycle of both creating printed objects with new and diverse functionality and modulating of physical characteristics and performance. Furthermore, at the current stage of development, the hardware and approach disclosed is well-suited as a tool for use in emerging areas of production such as in the generation of polymer composite objects that are functionally-graded.

Declaration of Competing Interest

The authors have filed a patent application related to this work.

Acknowledgments

This work was funded by the Laboratory Directed Research and Development (LDRD) program at the Pacific Northwest National Laboratory (PNNL). PNNL is operated by Battelle for the U.S. Department of Energy under Contract DE-AC05-76RLO 1830. We would like to thank Cortland

Johnson for assistance in the preparation of the graphic in Figure 1 and acknowledge the hardware design work by Rodrigo Guerrero and Kent Evans.

References

[1] S. Ford, M. Despeisse, Additive manufacturing and sustainability: an exploratory study of the advantages and challenges, Journal of Cleaner Production 137 (2016) 1573-1587.

[2] S.A.M. Tofail, E.P. Koumoulos, A. Bandyopadhyay, S. Bose, L. O'Donoghue, C. Charitidis, Additive manufacturing: scientific and technological challenges, market uptake and opportunities, Materials Today 21(1) (2018) 22-37.

[3] B. Brenken, E. Barocio, A. Favaloro, V. Kunc, R.B. Pipes, Fused filament fabrication of fiber-reinforced polymers: A review, Additive Manufacturing 21 (2018) 1-16.

[4] J. Gonzalez-Gutierrez, S. Cano, S. Schuschnigg, C. Kukla, J. Sapkota, C. Holzer, Additive Manufacturing of Metallic and Ceramic Components by the Material Extrusion of Highly-Filled Polymers: A Review and Future Perspectives, Materials 11(5) (2018).

[5] S.C. Ligon, R. Liska, J. Stampfl, M. Gurr, R. Mülhaupt, Polymers for 3D Printing and Customized Additive Manufacturing, Chemical Reviews 117(15) (2017) 10212-10290.

[6] R.T. Shafranek, S.C. Millik, P.T. Smith, C.-U. Lee, A.J. Boydston, A. Nelson, Stimuli-responsive materials in additive manufacturing, Progress in Polymer Science 93 (2019) 36-67.

[7] Z.C. Kennedy, J.F. Christ, K.A. Evans, B.W. Arey, L.E. Sweet, M.G. Warner, R.L. Erikson, C.A. Barrett, 3D-printed poly(vinylidene fluoride)/carbon nanotube composites as a tunable, low-cost chemical vapour sensing platform, Nanoscale 9(17) (2017) 5458-5466.

[8] R.D. Farahani, M. Dubé, D. Therriault, Three-Dimensional Printing of Multifunctional Nanocomposites: Manufacturing Techniques and Applications, Advanced Materials 28(28) (2016) 5794-5821.

[9] Z.C. Kennedy, D.E. Stephenson, J.F. Christ, T.R. Pope, B.W. Arey, C.A. Barrett, M.G. Warner, Enhanced anti-counterfeiting measures for additive manufacturing: coupling lanthanide nanomaterial chemical signatures with blockchain technology, Journal of Materials Chemistry C 5(37) (2017) 9570-9578.

[10] X. Wang, M. Jiang, Z. Zhou, J. Gou, D. Hui, 3D printing of polymer matrix composites: A review and prospective, Composites Part B: Engineering 110 (2017) 442-458.

[11] F. Peng, H. Jiang, A. Woods, P. Joo, E.J. Amis, N.S. Zacharia, B.D. Vogt, 3D Printing with Core–Shell Filaments Containing High or Low Density Polyethylene Shells, ACS Applied Polymer Materials 1(2) (2019) 275-285.

[12] T.P. D'Amico, C. Barrett, J. Presing, R. Patnayakuni, M. Pourali, A.M. Peterson, Harnessing irreversible thermal strain for shape memory in polymer additive manufacturing, Journal of Applied Polymer Science 136(47) (2019) 48239.

[13] E.L. Gilmer, D. Miller, C.A. Chatham, C. Zawaski, J.J. Fallon, A. Pekkanen, T.E. Long, C.B. Williams, M.J. Bortner, Model analysis of feedstock behavior in fused filament fabrication: Enabling rapid materials screening, Polymer 152 (2018) 51-61.

[14] A. D'Amico, A.M. Peterson, An adaptable FEA simulation of material extrusion additive manufacturing heat transfer in 3D, Additive Manufacturing 21 (2018) 422-430.

[15] F. Hermes, S. Bernhardt, D. Poppe, G. Schmitt, M. Pridoehl, G. Loehden, Maleic anhydride copolymers as soluble support material for fused deposition modelling (FDM) printer, Google Patents, 2014.

[16] D.V. Isakov, Q. Lei, F. Castles, C.J. Stevens, C.R.M. Grovenor, P.S. Grant, 3D printed anisotropic dielectric composite with meta-material features, Materials & Design 93 (2016) 423-430.

[17] RepRap, Diamond Hotend — RepRap. <https://reprap.org/mediawiki/index.php?title=Diamond_Hotend&oldid=183708>, 2018).

[18] <http://ordsolutions.com>, 2019 (accessed June 12, 2019).

[19] M.A. Skylar-Scott, J. Mueller, C.W. Visser, J.A. Lewis, Voxelated soft matter via multimaterial multinozzle 3D printing, Nature 575(7782) (2019) 330-335.

[20] J.A. Lewis, T.J. Ober, Microfluidic active mixing nozzle for three-dimensional printing of viscoelastic inks, U.S. Patent 10,071,350, 2018.

[21] M.A.H. Khondoker, A. Asad, D. Sameoto, Printing with mechanically interlocked extrudates using a custom bi-extruder for fused deposition modelling, Rapid Prototyping Journal 24(6) (2018) 921-934.

[22] M.A.H. Khondoker, N. Baheri, D. Sameoto, Tendon-Driven Functionally Gradient Soft Robotic Gripper 3D Printed with Intermixed Extrudate of Hard and Soft Thermoplastics, 3D Printing and Additive Manufacturing 6(4) (2019) 191-203.

[23] A. Garland, G. Fadel, Design and Manufacturing Functionally Gradient Material Objects With an Off the Shelf Three-Dimensional Printer: Challenges and Solutions, Journal of Mechanical Design 137(11) (2015).

[24] ISO 527-1:2012(E), Plastics — Determination of Tensile Properties, International Organization for Standardization, Switzerland, 2012.

[25] S. A. Gold, R. Strong, B. N. Turner, A review of melt extrusion additive manufacturing processes: I. Process design and modeling, Rapid Prototyping Journal 20(3) (2014) 192-204.

[26] M. Lin, N. Firoozi, C.-T. Tsai, M.B. Wallace, Y. Kang, 3D-printed flexible polymer stents for potential applications in inoperable esophageal malignancies, Acta Biomaterialia 83 (2019) 119-129.

[27] M. Alsharari, B. Chen, W. Shu, 3D Printing of Highly Stretchable and Sensitive Strain Sensors Using Graphene Based Composites, Multidisciplinary Digital Publishing Institute Proceedings, 2018, p. 792.

[28] Q. Chen, J.D. Mangadlao, J. Wallat, A. De Leon, J.K. Pokorski, R.C. Advincula, 3D Printing Biocompatible Polyurethane/Poly(lactic acid)/Graphene Oxide Nanocomposites: Anisotropic Properties, ACS Applied Materials & Interfaces 9(4) (2017) 4015-4023.

[29] N.G. Tanikella, B. Wittbrodt, J.M. Pearce, Tensile strength of commercial polymer materials for fused filament fabrication 3D printing, Additive Manufacturing 15 (2017) 40-47.

[30] P. Pötschke, D.R. Paul, Formation of Co-continuous Structures in Melt-Mixed Immiscible Polymer Blends, Journal of Macromolecular Science, Part C 43(1) (2003) 87-141.

[31] E. Oliaei, B. Kaffashi, S. Davoodi, Investigation of structure and mechanical properties of toughened poly(l-lactide)/thermoplastic poly(ester urethane) blends, Journal of Applied Polymer Science 133(15) (2016).

[32] F. Feng, L. Ye, Morphologies and mechanical properties of polylactide/thermoplastic polyurethane elastomer blends, Journal of Applied Polymer Science 119(5) (2011) 2778-2783.

[33] H.-Y. Mi, M.R. Salick, X. Jing, B.R. Jacques, W.C. Crone, X.-F. Peng, L.-S. Turng, Characterization of thermoplastic polyurethane/polylactic acid (TPU/PLA) tissue engineering scaffolds fabricated by microcellular injection molding, Materials Science and Engineering: C 33(8) (2013) 4767-4776.

[34] X. Jing, H.-Y. Mi, X.-F. Peng, L.-S. Turng, The morphology, properties, and shape memory behavior of polylactic acid/thermoplastic polyurethane blends, Polymer Engineering & Science 55(1) (2015) 70-80.

[35] B. Robertson, R.L. Thompson, T.C.B. McLeish, I. Robinson, Polymer extrudate-swell: From monodisperse melts to polydispersity and flow-induced reduction in monomer friction, Journal of Rheology 63(2) (2019) 319-333.

[36] A.M. Henderson, A. Rudin, Effects of die temperature on extrudate swell in screw extrusion, Journal of Applied Polymer Science 31(2) (1986) 353-365.

[37] W.W. Graessley, S.D. Glasscock, R.L. Crawley, Die swell in molten polymers, Transactions of the Society of Rheology 14(4) (1970) 519-544.

[38] R.I. Tanner, A theory of die-swell, Journal of Polymer Science Part A-2: Polymer Physics 8(12) (1970) 2067-2078.

[39] T.S. Natarajan, S.B. Eshwaran, K.W. Stöckelhuber, S. Wießner, P. Pötschke, G. Heinrich, A. Das, Strong Strain Sensing Performance of Natural Rubber Nanocomposites, ACS Applied Materials & Interfaces 9(5) (2017) 4860-4872.

[40] W. Bauhofer, J.Z. Kovacs, A review and analysis of electrical percolation in carbon nanotube polymer composites, Composites Science and Technology 69(10) (2009) 1486-1498.

[41] F. Du, J.E. Fischer, K.I. Winey, Effect of nanotube alignment on percolation conductivity in carbon nanotube/polymer composites, Physical Review B 72(12) (2005) 121404.

[42] E. Chang, A. Ameli, L.H. Mark, C.B. Park, Effects of uniaxial and biaxial orientation on fiber percolation in conductive polymer composites, AIP Conference Proceedings 1695(1) (2015) 020027.

[43] T. Villmow, P. Pötschke, S. Pegel, L. Häussler, B. Kretzschmar, Influence of twin-screw extrusion conditions on the dispersion of multi-walled carbon nanotubes in a poly(lactic acid) matrix, Polymer 49(16) (2008) 3500-3509.